SCIENTIFIC REPORTS

OPEN

SUBJECT AREAS:
OPTICAL MATERIALS
OPTICAL PHYSICS
OPTICS AND PHOTONICS
OPTICAL MATERIALS AND STRUCTURES

Received
20 July 2012

Accepted
17 September 2012

Published
7 November 2012

Correspondence and requests for materials should be addressed to H.D.S. (HDSun@ntu.edu.sg) or B.Z. (blzhang@ntu.edu.sg)

Radiation-Suppressed plasmonic open resonators designed by nonmagnetic transformation optics

Hongyi Xu, Xingjue Wang, Tianyuan Yu, Handong Sun & Baile Zhang

Division of Physics and Applied Physics, School of Physical and Mathematical Sciences, Nanyang Technological University, 21 Nanyang Link, Singapore 637371, Singapore.

How to confine light energy associated with surface plasmon polaritons (SPPs) in a physical space with minimal radiation loss whereas creating maximum interacting section with surrounding environment is of particular interest in plasmonic optics. By virtue of transformation optics, we propose a design method of forming a polygonal surface-plasmonic resonator in fully open structures by applying the nonmagnetic affine transformation optics strategy. The radiation loss can be suppressed because SPPs that propagate in the designed open structures will be deceived as if they were propagating on a flat metal/dielectric interface without radiation. Because of the nonmagnetic nature of the transformation strategy, this design can be implemented with dielectric materials available in nature. An experimentally verifiable model is subsequently proposed for future experimental demonstration. Our design may find potential applications in omnidirectional sensing, light harvesting, energy storage and plasmonic lasing.

Optical resonator design is on its own a sub-discipline of optical science, beginning from the basic Fabry–Pérot structure[1] to more recent and more sophisticated designs[2]: the distributed feedback resonator and the distributed Bragg reflector[3] for improved wavelength selectivity; the resonator made by photonic crystals[4,5] and metamaterials[6,7]; the micro disk resonator and spherical resonator[8–10], the resonator based on nanowires[11], nanorods[12], and even disordered media with random lasing phenomena[13] . Among all these varieties, metallic-dielectric surface plasmon polariton (SPP) resonator has recently attracted a lot of attention because of its capability to confine light energy in a subwavelength scale with great enhancement in light-matter interaction and light emission[14–18]. Applications include nanoscale lasers, enhanced light-emitting diodes, biochemical sensors and light energy harvesting devices.

A typical problem in SPP resonator design is how to reduce the radiation loss to the minimal, whereas the interaction section with the surrounding environment is still preserved at utmost. The former is in favor of achieving a high quality factor, whose value represents how well light can be confined in a resonator. The latter, on the other hand, is strongly desirable for omnidirectional sensing, light harvesting, and other applications of enhanced light-matter interaction. A lot of efforts have been made to reduce the radiation loss[15,18,19]. However, previous studies usually used metallic coating to isolate light energy in a metallic shell, which, unavoidably, will block most of the interacting section with the surrounding environment, and thus are not favorable for applications where signals or energy can come from multiple directions.

On the other hand, the textbook picture of SPP propagation[20] is a surface electromagnetic wave propagating on a flat metal/dielectric interface with no radiation loss whereas the interacting section with the environment is as large as the metal surface, being exactly the advantages desired in SPP resonators. This motivates us to explore the possibility of implanting the advantages of flat-interface SPP propagation into SPP resonators by wrapping the electromagnetic space around the metallic kernel of the resonator. The radiation loss can be suppressed because SPPs will be cheated as if they were propagating on a flat surface. The strategy we used is transformation optics, which controls the light propagation by creating an effective curved EM space based on the form invariance of Maxwell's equations[21–29]. To the best of our knowledge, it is the first time that transformation optics method is introduced into the design of high quality SPP resonators.

Results

Let us first discuss how to bend SPPs across a sharp corner with almost zero radiation loss. Previous studies have shown the efficient manipulation of guided light between two interfaces of photonic crystals through a sharp

corner[30], which has paved the way towards photonic crystal-based photonic circuits. Recently, a lot of efforts were paid in compact integration of on-chip plasmonic circuits for next-generation photonic components. However, there still lacks a feasible way to bend the propagation of SPPs across a sharp corner with extremely high transmission. Therefore this problem itself is of remarkable significance and is worth exploration. We first consider a flat metal/dielectric interface as shown in Fig. 1(a), where SPPs can propagate without radiation along the direction from point P_1 to point P_2. The spatial coordinates are also plotted to indicate the electromagnetic space geometrically. Note that since the field penetration through metal is usually negligible compared to the field extension in the dielectric layer[31,32], we only plot the spatial coordinates for the electromagnetic space in the dielectric layer above metal. In order to focus on the issue of radiation loss, we temporarily assume that there is no dissipative loss involved. In the simulation, we set the metal's permittivity $\varepsilon_m = -30.23$ (Ag at 826.6 nm when the dissipative loss is neglected) and the dielectric's permittivity $\varepsilon_d = 3.5$ (commercial glass SCHOTT N-LASF31A at 826.6 nm). Figure 1(e) shows the corresponding distribution of magnetic field amplitude ($|\mathbf{H}_z|$). To bend the propagation of SPPs, an intuitive way is to cut the electromagnetic space into two arms, along the dotted line BO in Fig. 1(a), and then bend the two arms around point O to form a right-angle sharp corner, as shown in Fig 1(b). Apparently, a gap of electromagnetic space will appear in the transition region T1. If the transition region T1 is simply filled with the same material as the glass, it will be expected that a lot of SPP energy will be scattered and reflected, giving rise to a very small transmission (about 14.57%), whose situation is shown in Fig. 1(f). This result is reasonable because SPPs propagating on P_1O and those propagating on OP_2 in Fig. 1(b) will have a serious momentum mismatch, which does not permit a high transmission through a sharp corner.

Recently, there have been proposals using transformation optics to effectively guide SPPs around bumps and corners[31–33]. However the produced transformation media in these methods in principle required magnetism (i.e. non-unitary permeability) and thus can only be realized by rescaling the permeability to unity when maintaining the refractive index unchanged[34]. For the type of conformal/quasi-conformal transformation that was originally proposed for the other polarization[35], this rescaling will not significantly affect the desired performance, because the produced gradient-refractive-index media have inherently minimal reflection and the problem of lateral shift for light rays[36] does not apply here. However, the conformal/quasi-conformal transformation cannot handle the ultra-sharp bending problems (bending a straight angle to be a right angle is fundamentally not conformal). For the type of non-conformal transformation, this rescaling approximation generally will lead to impedance mismatch, resulting in extra reflection in wave guiding. To demonstrate this extra reflection effect, we consider a transformation in Fig. 1(c) as an example, where the triangle AOB in Fig. 1(b) (The length L of AB is 1 in Fig. 1) is sheared to form the triangle AOB', and COB_r to form COB′. Point $B(B_r)$ is horizontally(vertically) sheared into the same point B′ so that the electromagnetic space surrounding the corner (i.e. $P_3B'P_4P_2OP_1$) is equivalent to the counterpart $P_3P_4P_2P_1$ in Fig 1(a). From the principle of transformation optics[21,22], the sheared regions require anisotropic permittivity $\bar{\bar{\varepsilon}}' = \bar{\bar{J}}\bar{\bar{\varepsilon}}_d\bar{\bar{J}}^T/\det(\bar{\bar{J}})$ and non-unitary permeability $\mu' = 1/\det(\bar{\bar{J}})$, where $\det(\bar{\bar{J}})$ is the determinant of Jacobean that measures the area changing ratio. Because the areas before/after transformation are different, $\det(\bar{\bar{J}})$ is non-unitary and hence the permeability μ′ is non-unitary. When μ′ is rescaled to 1, the two principal permittivity components in $\bar{\bar{\varepsilon}}'$ need to be inversely scaled to keep the refractive index unchanged, and become $\varepsilon_1=4.58$ and $\varepsilon_2=0.67$. The effect of impedance mismatch can be seen in Fig. 1(g): although there is large improvement of transmission (T=79.65%), some reflection can still be observed at transformation/non-transformation interfaces OA and OC. It should be noted that this example is proposed solely for the purpose of comparison, and a more realistic model will be discussed later.

We next consider the possibility of further improving the transmission of SPPs across the point O in Fig. 1(c). Since the propagation of SPPs is mainly along the metal/dielectric interface P_1OP_2, the outer boundary P_3BP_4 is actually flexible because of the evanescent nature of SPPs. This property is completely different from previous waveguide applications where all boundaries of transformation media need to be fixed once the waveguide shape is determined. With the extra freedom of altering the outer boundary, it is possible to eliminate impedance mismatch by choosing an area-preserved transformation as follows. Rather than being sheared horizontally as in Fig. 1(c), point B can be sheared along the line BB′ where BB′// AO, as it is shown in Fig. 1(d). With this area-preserved constraint, AOB is transformed to AOB′ (area AOB′ is equal to area AOB), and COB_r to COB′. The determinant of Jacobean $\det(\bar{\bar{J}})$ therefore becomes 1, leading to a unitary permeability μ′. The two principal permittivity components are $\varepsilon_1=9.16$ and $\varepsilon_2=1.36$ in bending regions T3. Because of the complete elimination of impedance

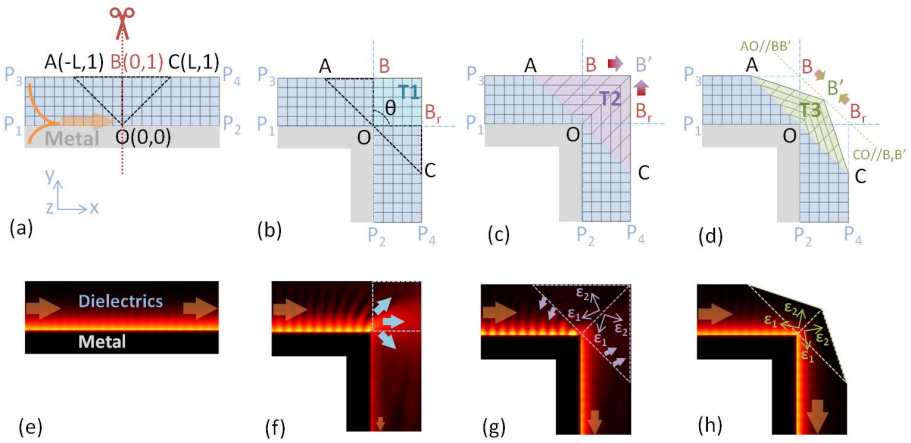

Figure 1 | (a) SPPs propagate on a flat metal/dielectric interface. The orange arrow indicates the propagation direction. (b) SPPs propagate across a right-angle corner in a nontransformed space. The position of point B_r is (1,0) and C is (1,-L). (c) The right-angle bending of SPPs propagation with permeability-rescaled transformation. Triangle AOB is transformed to AOB′, and COB_r to COB′. (d) The right-angle bending of SPPs propagation with area-preserved transformation. (e)–(h) The distribution of magnetic field amplitude $|\mathbf{H}_z|$ corresponding to (a)–(d), respectively. The two principal permittivity components are $\varepsilon_1=4.58$ and $\varepsilon_2=0.67$ in (g) and $\varepsilon_1=9.16$, $\varepsilon_2=1.36$ in (h). The length L of AB is 1 in all cases.

mismatch, a nearly-perfect transmission T=98.52% is shown in Fig. 1(h).

Now that we understand the mechanism of bending SPPs across a sharp corner, let us proceed to bend SPP propagation across multiple corners to form an SPP resonator. The bending angle for each corner satisfies $\theta=2\pi/p$ where p is the number of corners of the resonator. The circumference of resonator L_R [the length of $E_1E_2E_3E_4$ in Fig. 2(a)–(c)] is designed to satisfy the resonance condition $L_R=m\lambda_0/n_{eff}$, where m is the longitudinal mode number and $n_{eff}=[(\varepsilon_d\varepsilon_m)/(\varepsilon_d+\varepsilon_m)]^{1/2}$ is the effective refractive index. We use normalized freespace wavelength $\lambda_0=1$ and mode number m=25. A line source (the white dashed line in Fig. 2) for transverse magnetic wave is placed at the middle of an edge. The spatial coordinates of cases without transformation, with permeability-rescaled transformation and with area-preserved transformation are shown in Fig. 2(a), (b) and (c), with respective simulation results of the distribution of magnetic field $\mathbf{H}_z$ in Fig. 2(d), (e) and (f). In Fig. 2(d), the resonator without transformation, the one-round transmission is 0.02% as SPPs strongly scattered at corners. The resonator with permeability-rescaled transformation is shown in Fig. 2(e) with a final one-round transmission T=46.44%. In comparison, the resonator by area-preserved method in Fig. 2(f) possesses transmission 97.42%.

The variation on the shape of SPP resonator is also possible when the bending angle of SPP propagation is altered. For example, triangular cases are shown in Fig. 3(a)–(c). The one-round transmissions are 0.05%, 73.08% and 95.54% for cases without transformation, with permeability-rescaled transformation and with area-preserved transformation, respectively. The hexagonal cases are in Fig. 3(d)–(f), with one-round transmissions 0.13%, 43.00% and 98.59%, respectively. In the triangular case [Fig. 3(c)] where $\theta=120$ degree and $L=\sqrt{3}$, the two principle permittivity components are $\varepsilon_1=10.49$ and $\varepsilon_2=1.16$ in the transformation regions T3. The same values of ε_1 and ε_2 can be achieved in the hexagonal case [Fig. 3(f)] when $\theta=60$ degree and L=0.5.

The previous cases in Fig. 2(c), Fig. 3(c) and (f) demonstrate the possibility of using dielectrics to implement such resonators. Current metamaterial technologies have been able to achieve these permittivity components, especially at relatively low frequencies such as microwave and terahertz. However, to achieve these values at optical spectrum is still difficult. In order to push the resonator model into optical regime, we need to utilize another freedom of design, the anisotropic ratio which is defined as $R=\sqrt{\varepsilon_2/\varepsilon_1}$ ($\varepsilon_2<\varepsilon_1$). Apparently

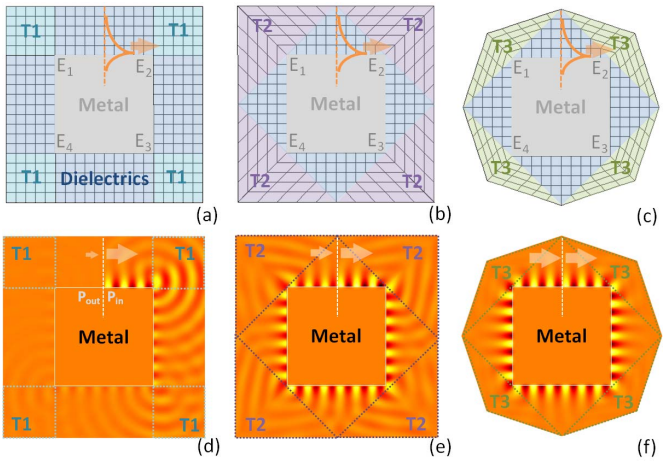

Figure 2 | The spatial coordinate of rectangular SPP resonators, (a) without transformation, (b) with permeability-rescaled transformation, and (c) with area-preserved transformation. The orange dashed lines mark the position of excitation source. (d)–(f) The distribution of the magnetic field $\mathbf{H}_z$ of (a)–(c), respectively.

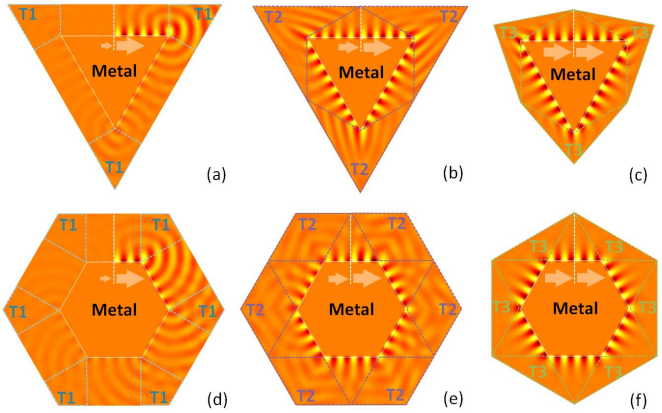

Figure 3 | The distribution of magnetic field $\mathbf{H}_z$ of triangular SPP resonators, (a) without transformation, (b) with permeability-rescaled transformation, and (c) with area-preserved transformation. The white dashed lines mark the position of excitation source, and the blue, purple, and green lines mark the transformation region. (d)–(f) The distribution of magnetic field $\mathbf{H}_z$ in hexagonal resonators.

R depends on the bending angle θ and the relative transformation length L [the length of AB in Fig. 1(a)]. A color map R(θ, L) is plotted in Fig. 4(a). It often occurs in practice that we are limited to a particular material or structure, with specific anisotropy. We can choose a proper value for R such that it can be achieved with targeted materials that we commonly used in practice.

Now let us begin the analysis of practical implementation with a specific anisotropy. Anisotropic permittivity can be realized by either natural birefringence materials[23,24,37] such as calcite, or artificial (form-birefringence) materials[38] like the silicon-air layered structure. We target to use the silicon-air layered structure to achieve the anisotropic ratio R required for a resonator. The minimum achievable R from the silicon-air layered structure is 0.53, as indicated by the white dotted line in Fig. 4(a). Therefore the region of R to the left of the dotted line is accessible for the silicon-air layered structure. By marking different shapes of resonators on the color map of R in Fig. 4(a), we can easily tell the feasibility of using the silicon-air layered structure to implement corresponding resonators. For example, resonators in shapes of pentagon, hexagon, octagon and dodecagon are all achievable with the targeted materials, while triangular and rectangular resonators are not achievable (indicated by dotted shapes). A hexagonal SPP resonator is presented as an

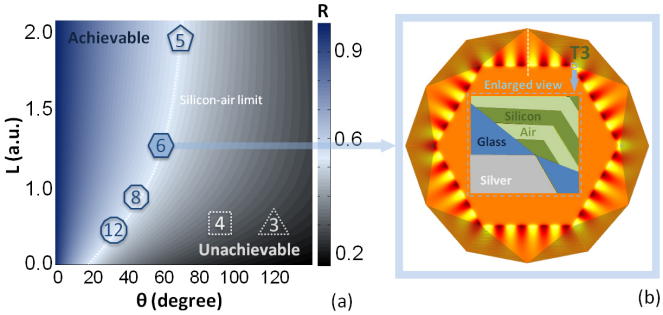

Figure 4 | (a) The anisotropic degree R as a function of the bending angle θ and the length L of line AB [Fig. 1(d)]. The white dashed curve mark the minimum anisotropic ratio R=0.53 of silicon-air layered structure. SPP Resonators are achievable by silicon-air layered structure (indicated by solid shapes) if R>0.53; and unachievable if R<0.53 (indicated by dashed shapes). (b) The distribution of magnetic field $\mathbf{H}_z$ of a hexagonal SPP resonator formed by silicon-air layered structure.

example in Fig. 4(b). The period of layers is chosen as $\lambda_0/20$, the filling factor is 0.5, and the orientation of layers is -2.64 degree with horizontal axis for the first bending region (inset, upper part). Silver is placed at the centre and SCHOTT glass at the edge for non-transformation regions. While in the simulation an evanescent wave is used for excitation, in real situation a plane wave, which can be decomposed into various spherical waves including high order evanescent modes, can also excite the resonance[39]. To further enhance excitation, some discrete scatterers can be distributed close to the resonator such that some enhanced evanescent waves generated from the scatterers can reach the resonator easily. As illustrated, the distribution pattern demonstrates little scattering, similar to that of the case without layered structure in Fig. 3(f), indicating a good performance of the silicon-air layered structure.

Discussion

The performance of a SPP resonator can be quantitative characterized by the quality factor, Q. In a SPP resonator Q is mainly determined by two factors: the radiation loss of SPPs and the dissipative loss from metal[18]. In previous sections we excluded the dissipative loss to focus on the issue of radiation loss. Now we discuss the influence of the realistic metallic loss on the resonator's performance. It is widely known that the dissipative loss can be effectively reduced by methods such as creating a shield layer between dielectrics and metals[19], or adopting superconducting metamaterials[40]. Besides these methods, an alternative solution is to operate the resonator at low temperatures. For example, previous experiments of SPP resonators were carried out at the temperature around 10 K[15,16]. Moreover, when active materials are involved, low temperature will increase the recombination rate of excitons for stimulated emission such that a lower lasing threshold can be achieved. Therefore, we assume the temperature at 10 K and recalculate the permittivity of the metal according to the conductivity rescaled method (see Methods). The resultant $\varepsilon_m = -30.23 + 0.0015i$ (826.6 nm) at T = 10 K. By definition the quality factor $Q=\omega E_s/P$[41], where E_s is the field energy stored in the resonator, and P is the power dissipated by resonator. In our simulation, $E_s=0.5(\varepsilon|\mathbf{E}|^2+\mu|\mathbf{H}|^2)$ and $P=P_{in} - P_{out}$ are the one-round energy stored and power loss including both dissipation and radiation. For the hexagonal SPP resonator with area-preserved transformation [Fig. 4(b)], Q is 8520 by simulation, comparable to values in full dielectric resonators (e.g. 3300[8], 8000[9] and 5500[10]). At room temperature, $\varepsilon_m = -30.23 + 1.59i$[42] and Q decreases to 336, as the result of the rise of metallic loss; yet it is still at the same order of magnitude compared to most SPP resonators up to date[15,43–45]. The comparison clearly demonstrates the advantage of area-preserved transformation based SPP resonator in radiation suppressing. There are still many possibilities to further improve the value of Q. For example, introducing a hybrid SPP structure[16,19] and applying a transformation to it. These methods for improvements are out of the scope of this paper.

In conclusion, we have introduced the nonmagnetic area-preserved transformation method into the design of a polygonal SPP resonator. Compared with traditional SPP resonators, the new design can achieve a large value of quality factor in a fully open structure by suppressing radiation loss of SPP propagation. The resonator, achievable by materials available in nature, can be potentially used in applications such as enhanced light-matter interaction, omnidirectional energy harvesting and high efficient nanoscale lasing.

Methods

The numerical simulations are performed by a commercial finite element method solver COMSOL Multiphysics (RF Module). The permittivity of silver and glass are set as -30.23 (lossless by assumption) and 3.5 at free space wavelength 826.6 nm in Figs. 1, 2 and 3, and as $-30.23+0.0015i$ (T = 10 K) and 3.5 in Fig. 4. The estimation of the imaginary part of the permittivity of silver at low temperature follows the conductivity rescaled method, i.e. the imaginary part is multiplied by a ratio of the room-temperature conductivity divided by the low-temperature conductivity[15,46].

1. Maiman, T. H. Stimulated Optical Radiation in Ruby. *Nature* **187**, 493–494 (1960).
2. Vahala, K. J. Optical microcavities. *Nature* **424**, 839–846 (2003).
3. Wang, S. Principles of distributed feedback and distributed bragg-reflector lasers. *IEEE J. Quantum Electron.* **10**, 413–427 (1974).
4. Park, H.-G. *et al.* Electrically Driven Single-Cell Photonic Crystal Laser. *Science* **305**, 1444–1447 (2004).
5. Ruan, Z. & He, S. Open cavity formed by a photonic crystal with negative effective index of refraction. *Opt. Lett.* **30**, 2308–2310 (2005).
6. Yan, W. & Shen, L. Open waveguide cavity using a negative index medium. *Opt. Lett.* **33**, 2806–2808 (2008).
7. Ginis, V., Tassin, P., Danckaert, J., Soukoulis, C. M. & Veretennicoff, I. Creating electromagnetic cavities using transformation optics. *New J Phys* **14**, 033007 (2012).
8. Chen, R., Ling, B., Sun, X. W. & Sun, H. D. Room Temperature Excitonic Whispering Gallery Mode Lasing from High-Quality Hexagonal ZnO Microdisks. *Advanced Materials* **23**, 2199–2204 (2011).
9. Ta, V. D., Chen, R. & Sun, H. D. Self-Assembled Flexible Microlasers. *Advanced Materials* **24**, OP60–OP64 (2012).
10. Chen, R., Van Duong, T. & Sun, H. D. Single Mode Lasing from Hybrid Hemispherical Microresonators. *Sci. Rep.* **2** (2012).
11. Huang, M. H. *et al.* Room-temperature ultraviolet nanowire nanolasers. *Science* **292**, 1897–1899 (2001).
12. Song, Q. H. & Cao, H. Improving Optical Confinement in Nanostructures via External Mode Coupling. *Physical Review Letters* **105**, 053902 (2010).
13. Cao, H. *et al.* Random laser action in semiconductor powder. *Physical Review Letters* **82**, 2278–2281 (1999).
14. Bozhevolnyi, S. I., Volkov, V. S., Devaux, E., Laluet, J. Y. & Ebbesen, T. W. Channel plasmon subwavelength waveguide components including interferometers and ring resonators. *Nature* **440**, 508–511 (2006).
15. Hill, M. T. *et al.* Lasing in metallic-coated nanocavities. *Nat Photon* **1**, 589–594 (2007).
16. Oulton, R. F. *et al.* Plasmon lasers at deep subwavelength scale. *Nature* **461**, 629–632 (2009).
17. Noginov, M. A. *et al.* Demonstration of a spaser-based nanolaser. *Nature* **460**, 1110–U1168 (2009).
18. Min, B. *et al.* High-Q surface-plasmon-polariton whispering-gallery microcavity. *Nature* **457**, 455–458 (2009).
19. Nezhad, M. P. *et al.* Room-temperature subwavelength metallo-dielectric lasers. *Nature Photonics* **4**, 395–399 (2010).
20. Raether, H. Surface Plasmons on Smooth and Rough Surfaces and on Gratings. *Springer-Verlag* (1988).
21. Pendry, J. B., Schurig, D. & Smith, D. R. Controlling electromagnetic fields. *Science* **312**, 1780–1782 (2006).
22. Leonhardt, U. Optical conformal mapping. *Science* **312**, 1777–1780 (2006).
23. Zhang, B., Luo, Y., Liu, X. & Barbastathis, G. Macroscopic Invisibility Cloak for Visible Light. *Phys. Rev. Lett.* **106**, 033901 (2011).
24. Chen, X. *et al.* Macroscopic invisibility cloaking of visible light. *Nat. Commun.* **2**, 1176 (2011).
25. Xu, H., Zhang, B., Yu, T., Barbastathis, G. & Sun, H. Dielectric waveguide bending adapter with ideal transmission: practical design strategy of area-preserving affine transformation optics. *J. Opt. Soc. Am. B* **29**, 1287–1290 (2012).
26. Xu, H. Y., Zhang, B., Barbastathis, G. & Sun, H. D. Compact optical waveguide coupler using homogeneous uniaxial medium. *J. Opt. Soc. Am. B* **28**, 2633–2636 (2011).
27. Yang, Y. *et al.* Optofluidic waveguide as a transformation optics device for lightwave bending and manipulation. *Nature Communications* **3**, 1162 (2012).
28. Chen, H., Chan, C. T. & Sheng, P. Transformation optics and metamaterials. *Nat Mater* **9**, 387–396 (2010).
29. Han, T. C., Qiu, C. W. & Tang, X. H. Adaptive waveguide bends with homogeneous, nonmagnetic, and isotropic materials. *Optics Letters* **36**, 181–183 (2011).
30. Lin, S.-Y., Chow, E., Hietala, V., Villeneuve, P. R. & Joannopoulos, J. D. Experimental Demonstration of Guiding and Bending of Electromagnetic Waves in a Photonic Crystal. *Science* **282**, 274–276 (1998).
31. Liu, Y., Zentgraf, T., Bartal, G. & Zhang, X. Transformational Plasmon Optics. *Nano Letters* **10**, 1991–1997 (2010).
32. Zhang, J., Xiao, S., Wubs, M. & Mortensen, N. A. Surface Plasmon Wave Adapter Designed with Transformation Optics. *ACS Nano* **5**, 4359–4364 (2011).
33. Huidobro, P. A., Nesterov, M. L., Martín-Moreno, L. & García-Vidal, F. J. Transformation Optics for Plasmonics. *Nano Letters* **10**, 1985–1990 (2010).
34. Cai, W., Chettiar, U. K., Kildishev, A. V. & Shalaev, V. M. Optical cloaking with metamaterials. *Nat. Photon.* **1**, 224–227 (2007).
35. Li, J. & Pendry, J. B. Hiding under the Carpet: A New Strategy for Cloaking. *Phys. Rev. Lett.* **101**, 203901 (2008).
36. Zhang, B., Chan, T. & Wu, B.-I. Lateral Shift Makes a Ground-Plane Cloak Detectable. *Phys. Rev. Lett.* **104**, 233903 (2010).
37. Chen, H. & Zheng, B. Broadband polygonal invisibility cloak for visible light. *Sci. Rep.* **2**, 255 (2012).

38. Zhang, J., Liu, L., Luo, Y., Zhang, S. & Mortensen, N. A. Homogeneous optical cloak constructed with uniform layered structures. *Opt. Express* **19**, 8625–8631 (2011).
39. Heifetz, A., Simpson, J. J., Kong, S.-C., Taflove, A. & Backman, V. Subdiffraction optical resolution of a gold nanosphere located within the nanojet of a Mie-resonant dielectric microsphere. *Opt. Express* **15**, 17334–17342 (2007).
40. Anagnostis Tsiatmas, V. A. F., Nikolay I. Zheludev. Plasmonics without losses? (the case for terahertz superconducting plasmonics). *arXiv* **1105**, 3045 (2011).
41. Yariv, A. Optical Electronics. *CBS College Publishing* (1985).
42. Palik, E. D. Handbook of Optical Constants of Solids. *Academic Press* (1998).
43. Kwon, S. H., Kang, J. H., Kim, S. K. & Park, H. G. Surface Plasmonic Nanodisk/Nanopan Lasers. *IEEE J. Quantum Electron.* **47**, 1346–1353 (2011).
44. Perahia, R., Alegre, T. P. M., Safavi-Naeini, A. H. & Painter, O. Surface-plasmon mode hybridization in subwavelength microdisk lasers. *Applied Physics Letters* **95**, 201114 (2009).
45. Zhu, X. L. *et al.* Confined Three-Dimensional Plasmon Modes inside a Ring-Shaped Nanocavity on a Silver Film Imaged by Cathodoluminescence Microscopy. *Physical Review Letters* **105** (2010).
46. Haynes, W. M. Handbook of Chemistry and Physics. *CRC Press* (2011).

Acknowledgments

The authors thank the financial support from Nanyang Technological University.

Author Contribution

HX, XW and TY performed the calculation and analyzed results, BZ and HS supervised the progress.

Additional information

Competing financial interests: The authors declare no competing financial interests.

How to cite this article: Xu, H., Wang, X., Yu, T., Sun, H. & Zhang, B. Radiation-Suppressed plasmonic open resonators designed by nonmagnetic transformation optics. *Sci. Rep.* **2**, 784; DOI:10.1038/srep00784 (2012).